Journal of Hazardous Materials 178 (2010) 233–242

Contents lists available at ScienceDirect

Journal of Hazardous Materials

journal homepage: www.elsevier.com/locate/jhazmat

Synthesis and the effect of calcination temperature on the physical–chemical properties and photocatalytic activities of Ni,La codoped $SrTiO_3$

Aizhong Jia[a,b], Xiuqing Liang[a], Zhiqian Su[a], Tan Zhu[b], Shuangxi Liu[a,*]

[a] Institute of New Catalytic Materials Science, College of Chemistry, Nankai University, Tianjin 300071, People's Republic of China
[b] College of Environmental Science and Engineering, Nankai University, Tianjin 300071, People's Republic of China

ARTICLE INFO

Article history:
Received 29 September 2009
Received in revised form 12 January 2010
Accepted 13 January 2010
Available online 18 January 2010

Keywords:
Photocatalysis
Sol–gel
Strontium titanate
Codoped
Visible light activity

ABSTRACT

A series of highly vis-light active Ni,La-codoped $SrTiO_3$ photocatalysts were successfully synthesized with sol–gel process. The characterization results show that the calcination temperature has a strong influence on the physical–chemical properties of as-synthesized photocatalysts. The surface area and porosity, even the initial adsorption rate for malachite green (MG), decreased with increasing calcination temperature. To evaluate the photocatalytic activities, the photodegradation of a water contaminant (MG) was carried out under visible light irradiation. The as-synthesized photocatalysts exhibited a high vis-light activity, and a 100% degradation of MG was observed for the Ni,La-$SrTiO_3$-*x* catalysts calcined at low temperature under visible light irradiation for 1 h, during which only 7% and 15% of MG was degraded for self-degrade and commercially available photocatalyst Degussa P25, respectively. The high vis-light activity is a result of the best combination of many properties, such as the intensive visible light response, the large surface area and pore volume and the high initial adsorption rate for substrate.

1. Introduction

As an efficient photocatalyst, strontium titanate ($SrTiO_3$) has been widely researched for the degradation of various organic contaminants, such as dyes [1–5] and other organic compounds [6,7], to solve environmental problems and for water splitting to produce clean energy [8–12]. A main drawback of the lack of photoresponse to the visible light, under which the $SrTiO_3$ cannot be effectively excited because of its wide band gap, limits its applications in solar light containing only 3% UV light. Therefore, numerous studies have attempted to extend the photoresponse of wide band gap photocatalysts, such as TiO_2 and $SrTiO_3$, towards the visible light to use solar light. A common method is modifying them by anion doping [13–17], metal doping [11,18–21] or generating oxygen deficiency [22].

In the 1980s, Domen et al. [9,12,23] found that NiO is an effective co-catalyst for photocatalytic decomposition of H_2O over photocatalyst of $SrTiO_3$. Recently, it has been reported that the visible light response can be effectively improved by doping $SrTiO_3$ with Ni^{2+} due to the forming of an electron donor level by Ni 3d orbits in the forbidden band to the conduction band [24]. However, the study on $SrTiO_3$ doped with Ni is still very few and only reported by Niishiro et al. [24]. It has also been proved that charge balance by codoping of another ion plays an important role in the photocatalytic activity [25,26]. It is known that La^{3+} has nearly the same ionic radius (0.115 nm) as Sr^{2+} (0.113 nm) and can replace Sr^{2+} in $SrTiO_3$ without producing a large lattice strain. Besides the photoresponse, the photocatalytic activity is also strongly affected by many other physical–chemical properties, such as particle size [27], crystal form [28,29], initial adsorption rate for substrate [30,31], surface area [32,33] and surface properties [34,35], which are changed remarkably according to different preparation and/or treatment procedure, during which the calcination temperature is the key factor in determining the above-mentioned.

Within this context, the present work aims to extend the photoresponse of $SrTiO_3$ towards visible light region by co-doping it with metal ions, namely nickel and lanthanum. The effect of calcination temperature on the physical–chemical properties and on photocatalytic activities of the synthesized catalysts has been investigated in detail. The photocatalytic activities were evaluated by studying the degradation of malachite green (MG), a water contaminant, under visible light irradiation.

2. Experimental

2.1. Preparation of photocatalysts

Ni,La-codoped $SrTiO_3$ powders were synthesized by a sol–gel process. A typical procedure was carried out as follows: 6.8 mL of tetrabutyl titanate was mixed with 10 mL of acetic acid glacial, and

* Corresponding author. Tel.: +86 22 23509005; fax: +86 22 23509005.
E-mail address: sxliu@nankai.edu.cn (S. Liu).

0304-3894/$ – see front matter © 2010 Elsevier B.V. All rights reserved.
doi:10.1016/j.jhazmat.2010.01.068

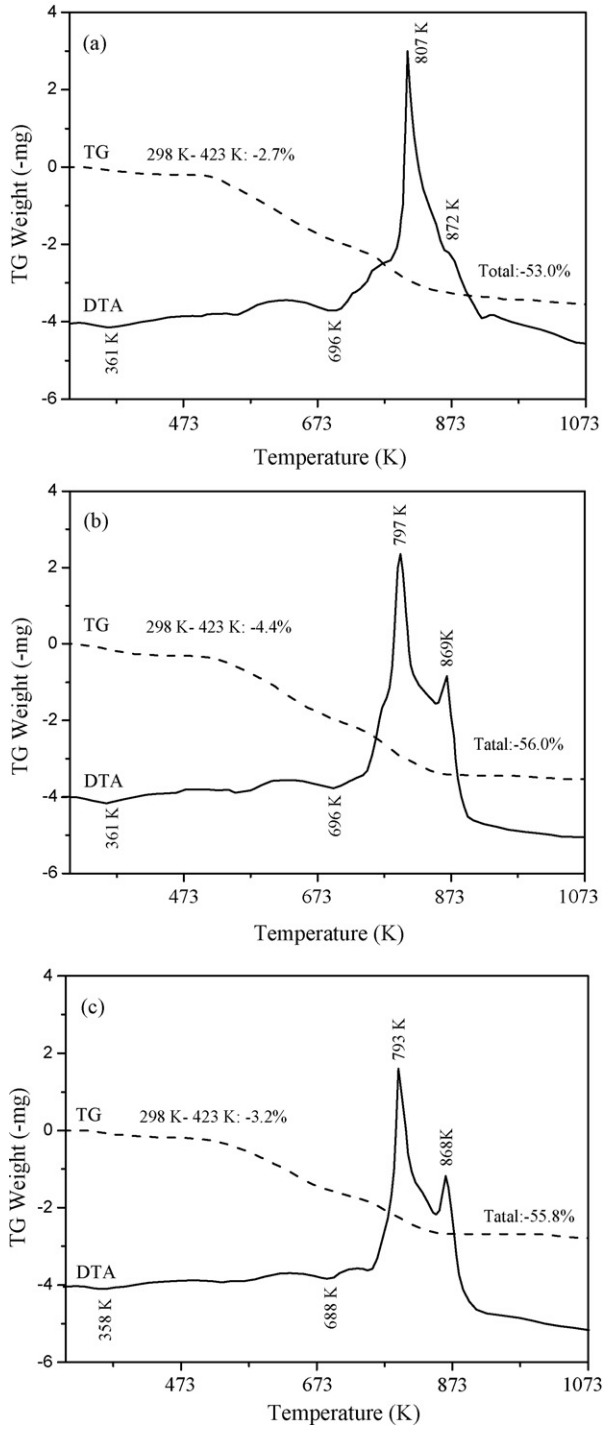

Fig. 1. TG/DTA curves of the xerogel precursor powders dried at 453 K: (a) Ni,La-SrTO-0; (b) Ni,La-SrTO-1.0; (c) Ni,La-SrTO-5.0.

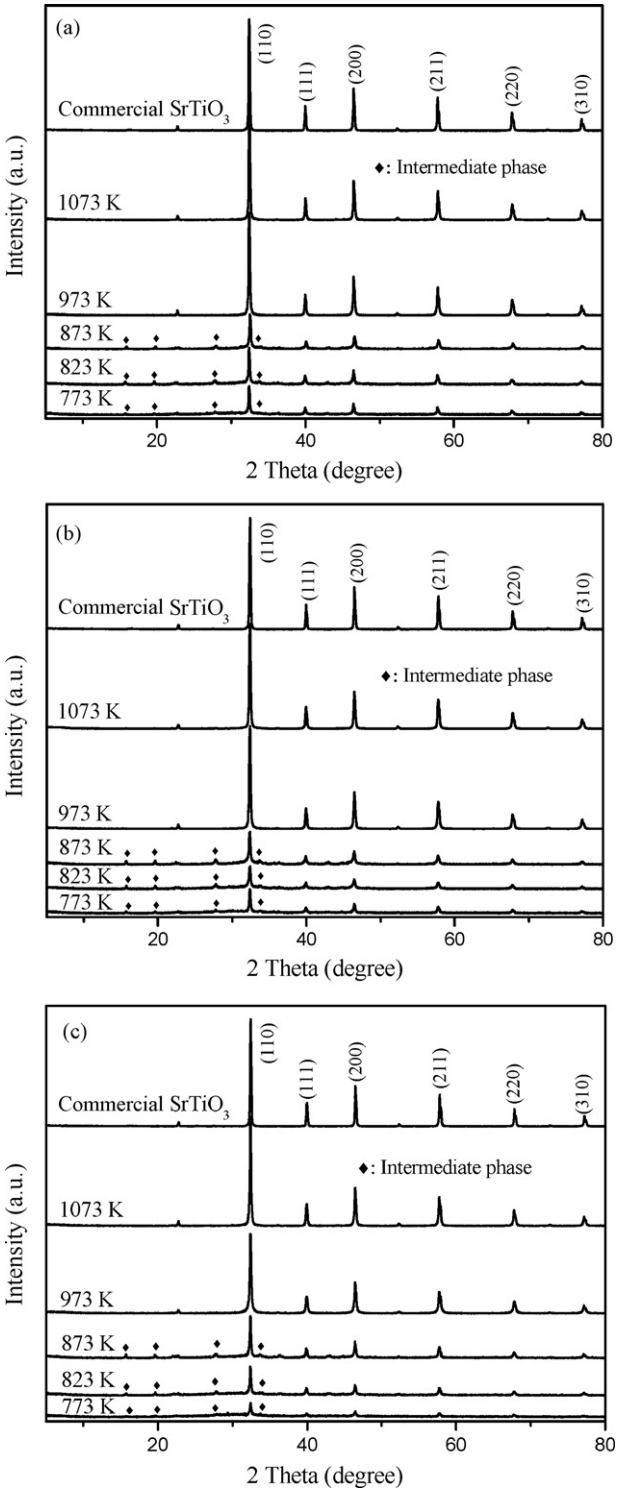

Fig. 2. XRD patterns of synthesized photocatalysts: (a) Ni,La-SrTO-0; (b) Ni,La-SrTO-1.0; (c) Ni,La-SrTO-5.0.

10 mL of water was added dropwise into the solution. The mixture was stirred until a clear solution (solution A) was obtained. A certain amount of La, Ni and Sr precursors was dissolved in 10 mL of water, and 8.4 g of citric acid in 10 mL of water was added dropwise (solution B). After stirring for 30 min at room temperature, solution B was added dropwise into solution A. The resulting solution was stirred for another 30 min at room temperature, and then it was heated to 338 K by water bath and kept at this temperature for 4 h in a closed system. And then most of water was evaporated slowly at this temperature in 4–5 h, the solution turned very viscous and it was thoroughly dried at 383 K for 12 h and at 453 K for another 12 h. The brown powder was obtained after milling. The photocatalysts of Ni,La-codoped $SrTiO_3$ were produced by calcinating the powder at 673 K for 6 h and then at the stipulated temperature for 24 h. The synthesized catalysts were marked as Ni,La-STO-*x*, where *x* denotes the mol percent of Ni and La corresponding to Ti, and the equivalent doping of Ni and La was used in this experiment. The nondoped $SrTiO_3$ was synthesized for comparative purposes using the same method.

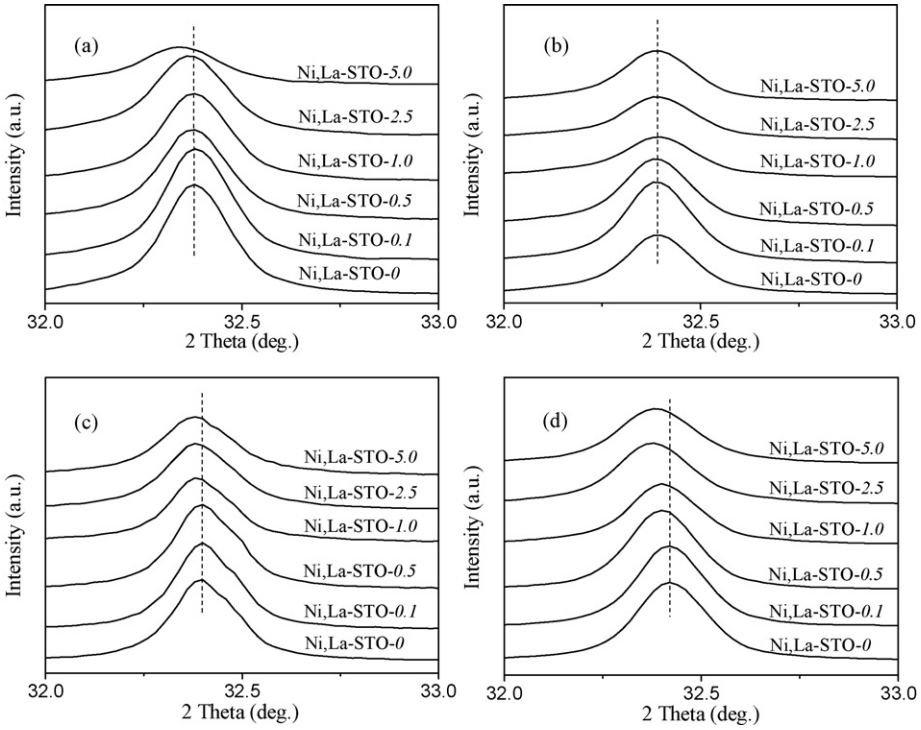

Fig. 3. The main peaks in XRD patterns of the synthesized Ni,La-STO-*x* series calcined at different temperatures: (a) 773 K; (b) 873 K; (c) 973 K; (d) 1073 K.

2.2. Characterization

Thermogravimetric analysis (TGA) and differential thermal analysis (DTA) of the precursor decomposition were simultaneously performed on a TG–DTA thermoanalyzer (PTC-10A) from 298 to 1073 K at a heating rate of 10 K min^{-1}. X-ray diffraction (XRD) patterns were collected on a Focus diffractometer (Bruker D8) with Cu Kα radiation (40 kV and 40 mA) at a scanning speed of 6° min^{-1}. The UV–vis diffuse reflectance spectra were measured at room temperature with a UV–vis spectrophotometer (Shimadzu 2550) in the range 200–800 nm. Scanning electron microscopy (SEM) images were recorded on an electron microscope (Shimadzu SS-550) operated at 25.0 kV. Nitrogen adsorption–desorption isotherms were determined at 77 K with a Micromeritics Tristar 3000 volumetric apparatus. Specific surface areas were calculated following the BET procedure. Pore diameters were estimated by applying the BJH method to the adsorption branch of the isotherm. Fourier transform infrared spectroscopic (FT-IR) analysis was conducted on a FT-IR spectrometer (Bruker VECTOR22) with a resolution of 1 cm^{-1} for the framework of materials. It was conducted using KBr wafers (1 wt.% catalyst mixed with 99 wt.% KBr).

2.3. Photocatalytic activity tests

The photocatalytic activities of the Ni,La-STO-*x* catalysts were evaluated by studying the photodegradation of MG under visible light irradiation. A 500 W xenon lamp was used as the light source and a UV filter plate was used to cut off the light of wavelength shorter than 400 nm. The suspension of 40 mL of 20 mg L^{-1} MG dye solution and 0.04 g of as-synthesized catalyst was stirred in 50 mL quartz reactor tube using a magnetic stirrer for 30 min before irradiation. After irradiation for 1 h, the degradation ratio of MG was measured using the UV–vis spectrophotometer at the maximum absorbance (617 nm) of MG. As a comparison, a blank experiment and a degradation reaction over commercial available photocatalyst Degussa P25 were also carried out under the same conditions.

Table 1
The structure properties of the synthesized photocatalysts and the initial adsorption rate (*h*) of MG on photocatalysts.

Photocatalyst	Calcination temperature (K)	Physical properties			Initial adsorption rate (*h*) (mol/g min) × 10^6
		S_{BET} (m^2/g)	Pore size (nm)	Pore vol. (cm^3/g)	
Ni,La-STO-0	773	17.7	11.5	0.061	9.04
Ni,La-STO-0	823	10.6	18.2	0.058	3.75
Ni,La-STO-0	873	7.9	31.9	0.047	2.45
Ni,La-STO-0	973	4.1	–	0.015	1.82
Ni,La-STO-0	1073	1.5	–	0.006	2.11
Ni,La-STO-1.0	773	17.8	14.9	0.054	6.31
Ni,La-STO-1.0	823	12.3	21.7	0.064	2.92
Ni,La-STO-1.0	873	11.0	29.7	0.068	1.98
Ni,La-STO-1.0	973	9.9	–[a]	0.046	1.48
Ni,La-STO-1.0	1073	3.2	–	0.021	1.53
Ni,La-STO-5.0	773	13.1	10.9	0.040	3.11
Ni,La-STO-5.0	823	11.5	18.5	0.046	1.96
Ni,La-STO-5.0	873	11.2	27.1	0.050	1.53
Ni,La-STO-5.0	973	9.2	32.4	0.045	1.24
Ni,La-STO-5.0	1073	5.7	–	0.034	1.07

[a] Hierarchical pore distribution.

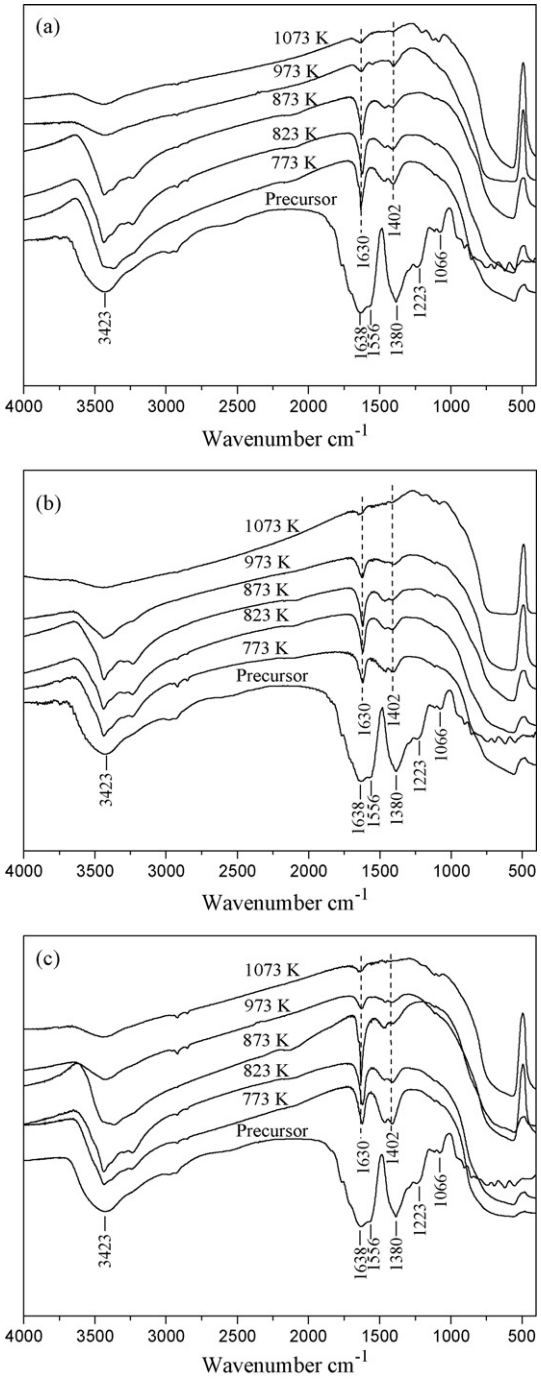

Fig. 4. FT-IR spectra of the synthesized photocatalysts and their xerogel precursors dried at 453 K: (a) Ni,La-SrTO-0; (b) Ni,La-SrTO-1.0; (c) Ni,La-SrTO-5.0.

The photocatalysts were recovered by centrifugation and dried at 373 K for 4 h.

3. Results and discussion

3.1. Characterization

3.1.1. TG/DTA analyses

The simultaneous TG/DTA analyses of the xerogel precursor powders containing different amount of Ni and La and dried at 453 K were carried out to study the thermal behavior, including the decomposition temperature and the corresponding weight loss, and the results are displayed in Fig. 1. The TG curves display a significant weight loss of more than 50% for all xerogel precursors below 873 K, and show three mass loss steps. The first one is ascribed to the dehydration which can be seen through an endothermic peak at about 361 K in the DTA curve. The second one is attributed to the decomposition of organic compounds corresponding to the endothermic peak at around 696 K in the DTA curve. The last step of mass loss is due to the combustion of organic compounds and/or

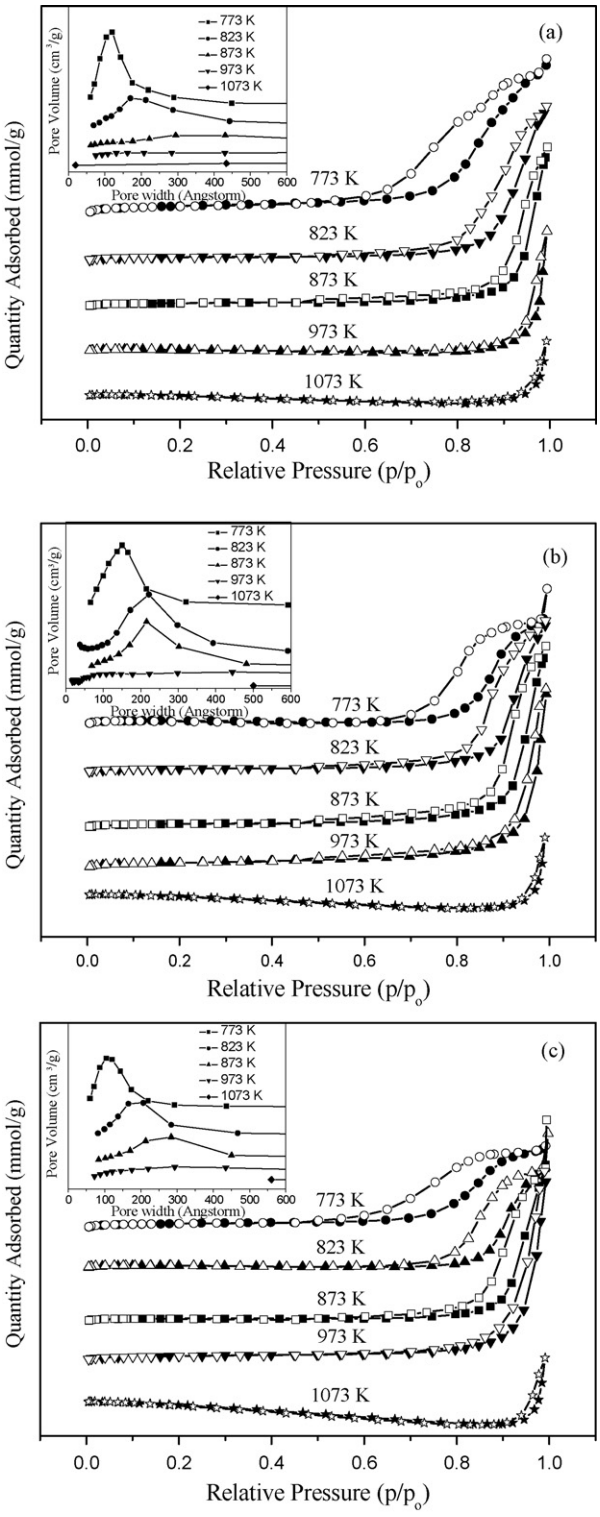

Fig. 5. N_2 adsorption–desorption isotherms and pore size distribution profiles (insets) of the synthesized photocatalysts: (a) Ni,La-SrTO-0; (b) Ni,La-SrTO-1.0; (c) Ni,La-SrTO-5.0.

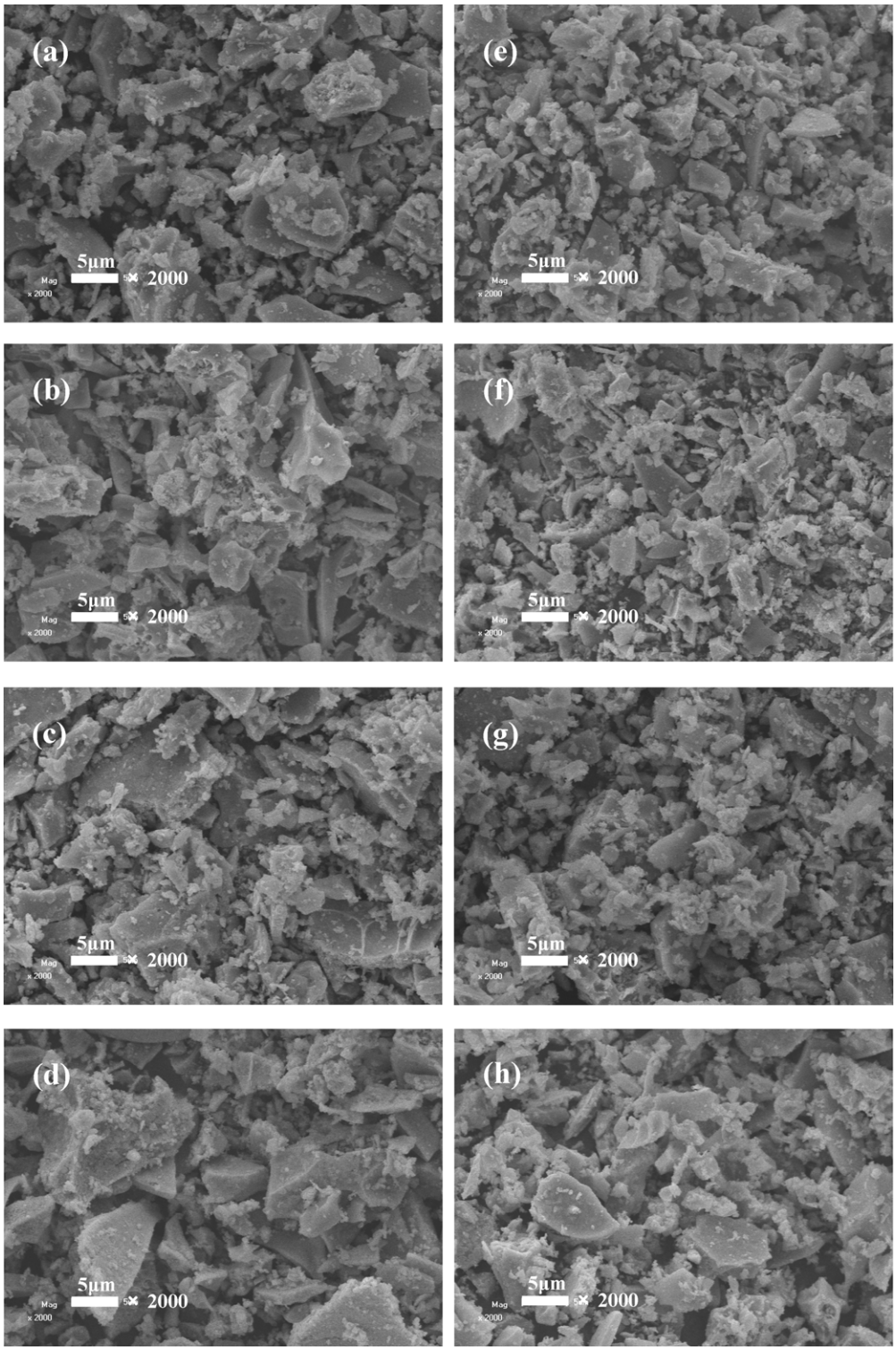

Fig. 6. SEM images of the synthesized photocatalysts of Ni,La-SrTO-0 (left-hand side) and Ni,La-SrTO-1.0 (right-hand side) calcined at different temperatures: (a and e) 773 K; (b and f) 873 K; (c and g) 973 K; (d and h) 1073 K.

the carbon formed via decomposition of organic compounds as suggested by the exothermic peak around 800 K in the DTA curve. So, in this work, the investigation on the effect of calcination temperature was conducted at temperature no lower than 773 K. It should be noted that the intensity of the exothermic peak at about 870 K was obviously increased when some Ni and La ions were added in the xerogel precursor. It can be attributed to the involvement of more cation vacancies in the equilibration reactions at high temperature in the case of donor doped material [36] when some ions were doped into the lattice of $SrTiO_3$.

3.1.2. X-ray diffraction analyses

The crystallinities of the obtained Ni,La-STO-*x* series were examined by XRD. The XRD patterns of Ni,La-STO-*x* series as compared to the commercial $SrTiO_3$ are shown in Fig. 2. The intensity of diffraction peaks increased with the increase of calcination temperature.

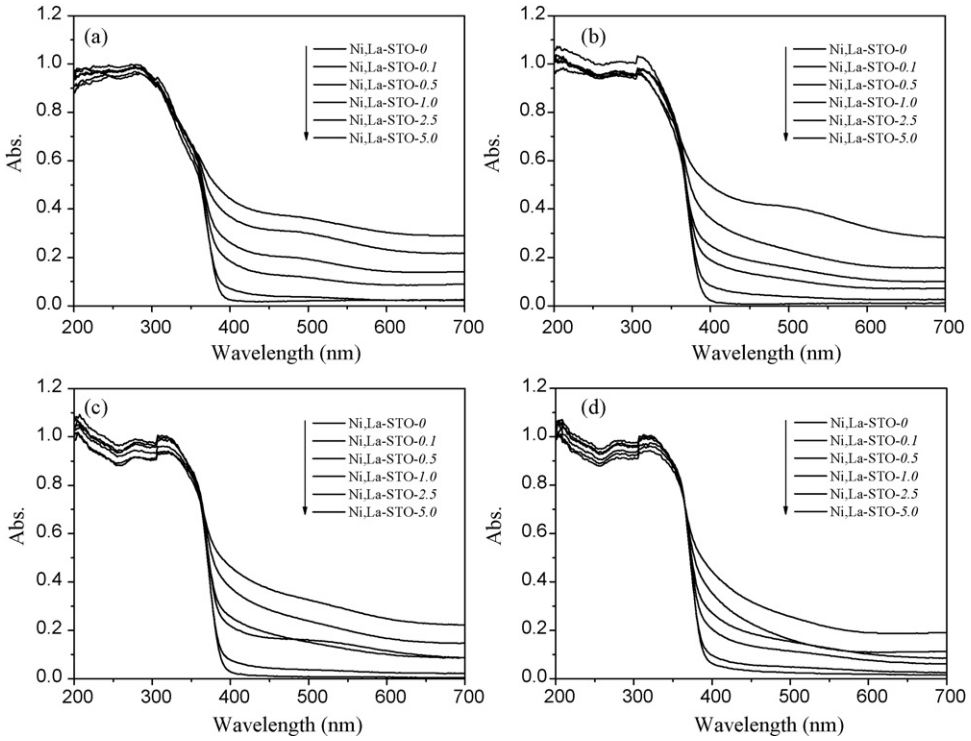

Fig. 7. UV–vis diffuse reflectance spectra of the synthesized Ni,La-STO-*x* series calcined at different temperature: (a) 773 K; (b) 873 K; (c) 973 K; (d) 1073 K.

The dominant peaks at about 32.4°, 39.9°, 46.4°, 57.8°, 67.8° and 77.2° represent the $SrTiO_3$ (1 1 0), (1 1 1), (2 0 0), (2 1 1), (2 2 0) and (3 1 0) surfaces [4], respectively, indicating that all the synthesized catalysts possess a perovskite structure, in spite of some weak peaks attributed to the intermediate phase found in the XRD patterns of catalysts calcined below 873 K. Furthermore, no peaks due to the other impurity appear in XRD patterns, indicating that doping of Ni and La has no obvious negative effect on the formation of perovskite structure.

Fig. 3 shows the main peak in the XRD patterns of Ni,La-STO-*x* series. In contrast to the nondoped $SrTiO_3$ series, the Ni,La-STO-*x* series show broad and weak diffraction peaks, which are probably due to the small sizes of $SrTiO_3$ crystals in the catalyst. It was also found that the peaks of Ni,La-STO-*x* shifted to lower angles compared to those of nondoped $SrTiO_3$, especially for the catalysts calcined at higher temperatures. This suggests that Sr^{2+} ions, with ionic radius of 0.113 nm in the lattice, were replaced by La^{3+} ions (0.115 nm), revealing a larger distortion and more defects were induced by doping the photocatalysts with Ni^{2+} and La^{3+} ions when the materials were calcined at higher temperatures.

3.1.3. FT-IR spectroscopy

Fig. 4 exhibits the FT-IR spectra of the catalysts doped with different amount of dopants and calcined at different temperature as well as their precursors. The absorption around 3423 cm^{-1} is assigned to the stretching vibration of lattice hydroxyls (either Ti–OH perturbed by nearby Sr atoms or Sr–OH groups) and naturally absorbed surface water whereas the peak around 1630 cm^{-1} can be assigned to the bending vibration of –OH [37,38]. The intensities of these peaks were observed to decrease with the increase in calcination temperature. For the catalyst calcined at 1073 K, the peaks almost disappeared. This demonstrates that more and more Ti–O–Sr and/or Ti–O–Ti bands had been formed via the dehydration reaction between Sr–OH and/or Ti–OH groups when the materials were calcined at the higher temperature. The shoulder appearing below 1000 cm^{-1} in the spectra of synthesized photocatalysts corresponds to the $SrTiO_3$ crystal lattice vibrations [17] and its intensity obviously increased with the increase in calcination temperature, indicating the formation of high crystallinity perovskite structure at high temperature.

In the spectra of precursors, the infrared spectral features appeared at 1380, 1223, 1066 cm^{-1} and at below 1000 cm^{-1} are attributed to the vibrations of C–H, C–C, and C–O of the residual organic compounds after baking at 453 K for 12 h. The complexation of Ti and Sr metallic cations can be analyzed by the vibrations at 1638, 1556 and 1380 cm^{-1}. The vibration at 1638 cm^{-1} is characteristic of a COO^- stretching mode for a unidentate complex and the vibrations at 1556 and 1380 cm^{-1} are related to a COO^- stretching mode for a bidentate complex [17,39].

3.1.4. N_2 adsorption–desorption isotherms

The effect of calcination temperature on the porous structure of as-synthesized catalysts was determined by nitrogen sorption. Fig. 5 presents the N_2 adsorption–desorption isotherms and the Barret–Joyner–Halenda (BJH) pore size distribution curves (insets). It is clearly seen that the isotherms of the catalysts calcined at low temperature (773 K) are type IV, indicating the existence of well-developed mesopores in their assembled frameworks [4]. With the increase in calcination temperature, the isotherms were transformed from type IV to type II, indicating that its pore structure was enlarged from mesopore to macropore, as confirmed by a very broad and right-shift pore size distribution, as shown in Fig. 5 (insets). Comparing the pore distributions, it can be found that the pores were broadened with increasing calcination temperature and thoroughly collapsed at 1073 K. This can be explained by the fact that the high temperature is favorable to the formation of dense phase and to the dehydration reaction between –OH groups, resulting in more Ti–O–Sr and/or Ti–O–Ti bands formation which is in good agreement with the results of FT-IR spectra discussed earlier. By comparing the average pore size (Table 1) and the pore size distribution of the catalysts doped with different amount of dopants (insets of Fig. 5a–c) it was found that the mesoporous structure

was still kept in the case of doped catalysts, whereas the mesostructure totally collapsed in the case of nondoped $SrTiO_3$ when calcined at 873 K, indicating that the doping of Ni and La increases the framework stability.

3.1.5. SEM images

The morphologies of nondoped $SrTiO_3$ and Ni,La-doped $SrTiO_3$ powders were studied using SEM. The SEM images of Ni,La-STO-0 series and Ni,La-STO-1.0 series exhibited in Fig. 6 show that both the catalysts possess anomalous morphology. It seems that the particle sizes of the doped catalysts were smaller than those of the nondoped $SrTiO_3$ in general. This is attributed to the fact that many crystal defects have been formed when the dopant ions occupy regular lattice sites inside and/or on the surface of $SrTiO_3$. As a result, the increase of the surface defect inhibits the growth of the crystal, which has also been reported in previous work [40,41]. The decrease of particle size would enhance the photocatalytic activities of the catalysts via increasing the active reaction sites by enlarging the surface area and decreasing the recombination of the photo-generated electrons and holes.

3.1.6. UV–vis diffuse reflectance spectra

Fig. 7 displays the UV–vis diffuse reflectance spectra of nondoped $SrTiO_3$ and Ni,La-codoped $SrTiO_3$ catalysts. As can be seen from Fig. 7, doped catalysts exhibit an absorption tail extending from UV to the visible region. With the increase of dopants, the photoabsorption of the catalysts in the visible region increased rapidly. In the case of Ni,La-codoped $SrTiO_3$ series, especially for the catalysts calcined at lower temperature and doped with high content of dopants (5%), a new broad absorption peak around 520 nm was observed in UV–vis diffuse reflectance spectra. It has been reported that the absorption band around 520 nm is attributed to a transition due to the level formed by Ni^{3+} ions [24,42]. The absorption intensity for the as-synthesized catalysts in this work was weaker than that of the reported results [24], indicating that the formation of Ni^{3+} ions has been evidently suppressed by codoping of La^{3+} ions. The broad absorption band transforms to an absorption tail when the catalysts were calcined at higher temperature, indicating that the formation of Ni^{3+} ions was inhibited at high temperature.

3.2. Catalytic properties

3.2.1. Adsorption kinetics

A study of kinetics of adsorption for MG is desirable as it provides the initial adsorption rate of the photocatalysts, which is important to their efficiency. The results for MG adsorption on Ni,La-STO-0, Ni,La-STO-1.0 and Ni,La-STO-5.0, which were calcined at 773 K, are shown in Fig. 8. The validity of adsorption kinetic model can be checked by the linearized plot. If it is applicable, the plot of t/q_t versus t should show a linear relationship. As shown in Table 2, the coefficient of determination values (R^2: 0.9560–0.9967) obtained from the pseudo-second-order kinetic model are higher than those obtained from the pseudo-first-order kinetic model (R^2: 0.8961–0.9886) and also the estimated q_e values from the pseudo-second-order model are more accurate. Both of them indicate that pseudo-second-order kinetic model is more applicable for the adsorption of MG on photocatalysts. Therefore, the pseudo-second-order model was selected, which is expressed as $dq_t/dt = k_2(q_e - q_t)^2$. As described in the work [43], the above-mentioned equation can be integrated to give $t/q_t = 1/k_2q_e^2 + t/q_e$, where q_e and q_t are the amount of MG adsorbed (mol g^{-1}) at equilibrium and at time t (min), respectively, and k_2 is the pseudo-second-order rate constant of adsorption (g mol^{-1} min^{-1}). The initial adsorption rate, h (mol g^{-1} min^{-1}) is expressed as $h = k_2q_e^2$, and the h values were calculated and listed in Table 1, from which it can be concluded that the initial adsorption rate evidently decreased with the increase in calcination temperature and the increase in dopant content. This trend can be attributed to the decrease in surface area and in the density of surface –OH groups with increase in calcination temperature, and the electrostatic repulsion between the metal cations and the cationic dye of MG.

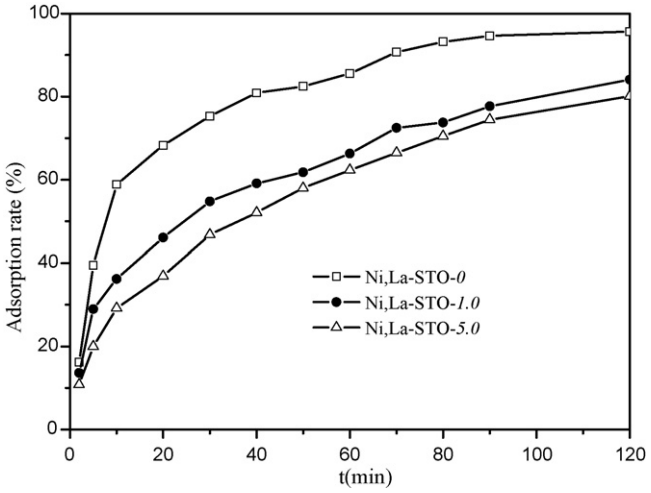

Fig. 8. The adsorption of MG on catalysts calcined at 773 K of Ni,La-SrTO-0, Ni,La-SrTO-1.0 and Ni,La-SrTO-5.0.

Table 2
Kinetic model parameters for the adsorption of MG on the prepared photocatalysts (q_e: mol g^{-1}; k_1: min^{-1}; k_2: g mol^{-1} min^{-1}).

Photocatalyst	Calcination temperature (K)	$q_{exp} \times 10^5$	Pseudo-first-order			Pseudo-second-order		
			$q_e \times 10^5$	k_1	R^2	$q_e \times 10^5$	$k_2 \times 10^{-2}$	R^2
Ni,La-STO-0	773	10.80	6.99	0.030	0.9705	11.58	6.74	0.9967
Ni,La-STO-0	823	9.02	7.47	0.020	0.9450	9.87	3.84	0.9752
Ni,La-STO-0	873	8.53	7.53	0.016	0.9661	9.40	2.77	0.9674
Ni,La-STO-0	973	7.03	6.20	0.017	0.9576	7.55	3.19	0.9581
Ni,La-STO-0	1073	6.13	5.35	0.020	0.9604	6.77	4.60	0.9665
Ni,La-STO-1.0	773	10.30	8.56	0.020	0.9717	11.29	4.95	0.9808
Ni,La-STO-1.0	823	9.21	8.63	0.020	0.9426	10.51	2.64	0.9642
Ni,La-STO-1.0	873	8.51	7.88	0.014	0.9478	9.35	2.26	0.9663
Ni,La-STO-1.0	973	6.45	5.76	0.013	0.9872	7.01	3.01	0.9677
Ni,La-STO-1.0	1073	5.25	4.50	0.017	0.9338	5.37	5.30	0.9560
Ni,La-STO-5.0	773	9.96	9.39	0.021	0.9581	10.50	2.82	0.9771
Ni,La-STO-5.0	823	8.43	7.88	0.015	0.9462	9.37	2.23	0.9650
Ni,La-STO-5.0	873	6.81	6.24	0.019	0.9132	7.05	3.07	0.9649
Ni,La-STO-5.0	973	5.17	4.81	0.015	0.8961	5.36	4.31	0.9678
Ni,La-STO-5.0	1073	2.52	2.25	0.023	0.9108	2.81	13.55	0.9824

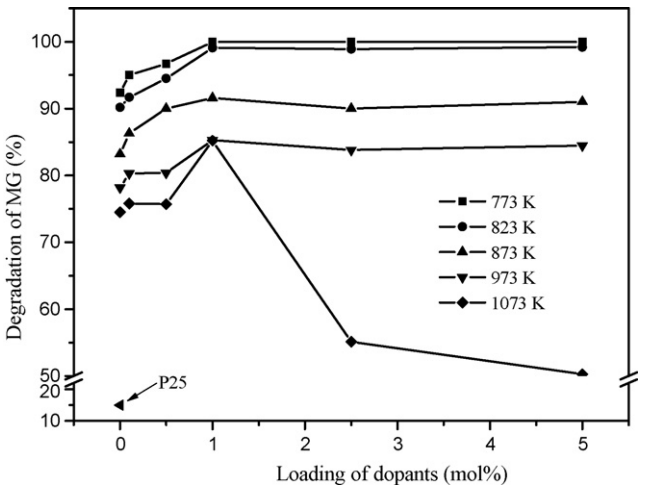

Fig. 9. The degradation of MG over synthesized photocatalysts doped with different amount of Ni and La and calcined at different temperature under visible light irradiation for 1 h.

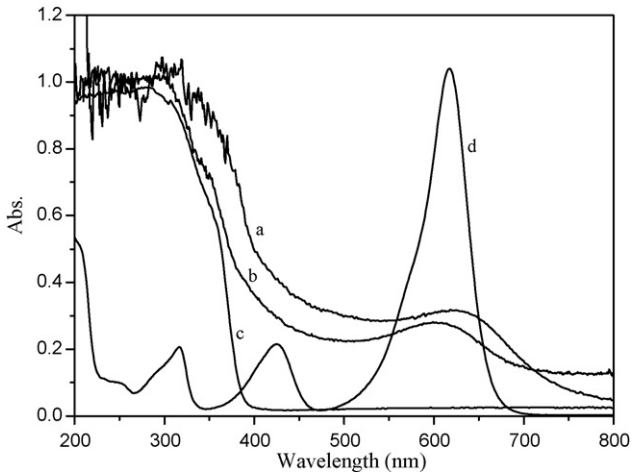

Fig. 10. UV–vis diffuse reflectance spectra of (a) MG-adsorbed $SrTiO_3$, (b) MG-adsorbed doped $SrTiO_3$, (c) nondoped $SrTiO_3$, and (d) MG in water solution.

3.2.2. Photocatalytic activities

The photocatalytic activities of nondoped $SrTiO_3$ and Ni,La-STO-*x* catalysts were evaluated in the MG degradation reaction in aqueous solution under visible light irradiation for 1 h, under which the self-degradation of MG in the absence of any catalysts was only 7%. The percentages of MG degradation versus the Ni and La content in Ni,La-STO-*x* series catalysts calcined at different temperature are shown in Fig. 9. It is found that all the synthesized catalysts have a much higher activity than that of commercially available photocatalyst Degussa P25, with which the degradation of MG was only 15%. Fig. 9 shows that the catalysts calcined at 773 K showed the highest photocatalytic activity (100% degradation of MG for Ni,La-STO-*x* ($x > 1.0$)) as compared to those calcined at higher temperatures. It is surprising that the nondoped $SrTiO_3$, which is almost nonactive in the visible region, also gave high degradation of MG. This can be explained according to the sensitization mechanism of photocatalysis. The MG molecules adsorbed on the catalysts can be excited by visible light photons [44,45]. The electron from the excited dye molecule is rapidly injected into the conduction band of the $SrTiO_3$, and the cation radical formed at the surface quickly undergoes degradation according to the following reactions:

$$MG + h\nu \rightarrow MG^* \quad (1)$$

$$MG^* + SrTiO_3 \rightarrow MG^+ + SrTiO_3(e^-) \quad (2)$$

$$SrTiO_3(e^-) + O_2 \rightarrow SrTiO_3 + O_2^- \quad (3)$$

$$MG^+ \rightarrow \text{Degradation of } MG^+ \quad (4)$$

The UV–vis diffuse reflectance spectra of MG-adsorbed $SrTiO_3$, MG-adsorbed doped $SrTiO_3$ and nondoped $SrTiO_3$ are shown in Fig. 10. For comparison, the solution spectrum of MG in water is also shown. The MG-adsorbed $SrTiO_3$ and MG-adsorbed doped $SrTiO_3$ display a very broad absorption in the 200–750 nm region, whereas, the nondoped $SrTiO_3$ and the MG in aqueous solution display different absorption bands. Such an extended coverage of MG-adsorbed $SrTiO_3$ in the visible region makes it possible to utilize most of the energy from visible light. So the nondoped $SrTiO_3$ also exhibits a high photocatalytic activity under visible light irradiation. However, the photocatalytic activities of all synthesized catalysts decreased with the increase in calcination temperature. This can be attributed to the obvious decrease in surface area and in initial adsorption rate as a result of calcination at higher temperature as shown in Table 1.

As shown in Fig. 9, there is an optimum doping amount of Ni and La for the visible light activity. Although the Ni,La-STO-5.0 series have the highest absorption in the visible light region (see Fig. 7), the degradation reaction over them gives a lower degradation rate than that of Ni,La-STO-1.0 series, which displays a lower absorption in the visible light region. Especially in the case of photocatalysts calcined at 1073 K, the activity decreased remarkably when the doping amount of Ni and La was higher than 1.0%. A similar phenomenon has also been reported by Miyauchi et al. [46], and it was ascribed to the result of creating more defects and/or large lattice distortion when the photocatalysts were doped with excess amount of metal ions. The crystal lattice of as-synthesized catalysts calcined at high temperature (given in Fig. 3) show a larger distortion when doping a higher amount of Ni and La cations, whereas, it is not notable for the catalysts calcined at low temperature. So the decrease in photocatalytic activities of photocatalysts calcined at high temperature may be assigned to the large lattice distortion in a certain extent. Furthermore, the evident decrease in surface area and the decrease in initial adsorption rate (as shown in Table 1) are other key factors for the decrease of visible light activity. For the special phenomena of catalysts calcined at 1073 K, it can be explained as the following. Firstly, for the dopant loading range from 0 to 1.0%, the increase in dopant loading led to an increase in both the specific surface area and the visible light response but to a decrease in the initial adsorption rate. In this loading range, the increase in the photocatalytic activity due to the positive effect of the increase of specific surface area and visible light response might exceed the negative effect of the decrease in initial adsorption rate. Secondly, for the dopant loading range from 1.0 to 5.0%, although the surface area and the visible light response increase with the increase of dopant loading, the negative effect of the reduction of the initial adsorption rate is dominant. So it seems reasonable to believe that the highest visible light activity is a result of the best combination of many properties of the synthesized photocatalysts. Fig. 11 illustrates the UV–vis spectra of MG solutions at different visible light illumination time over the catalyst of $SrTiO_3$-1.0 calcined at 773 K. The maximum absorbance of MG solution decreased markedly with a prolongation in the illumination time as shown in Fig. 11. This indicates that the MG has been degraded effectively over the prepared catalyst under visible light irradiation.

The stabilities of the synthesized Ni,La-STO-1.0 series catalysts calcined at different temperature have also been investigated and the results for four runs are given in Fig. 12. It is interesting to note that the catalysts calcined at lower temperatures were more stable and the degradation of MG for the catalyst calcined

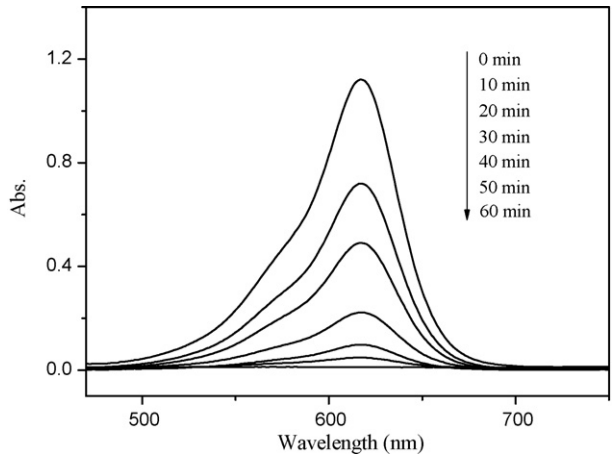

Fig. 11. UV–vis spectra of the MG solutions at different visible light illumination time over the catalyst of $SrTiO_3$-1.0 calcined at 773 K.

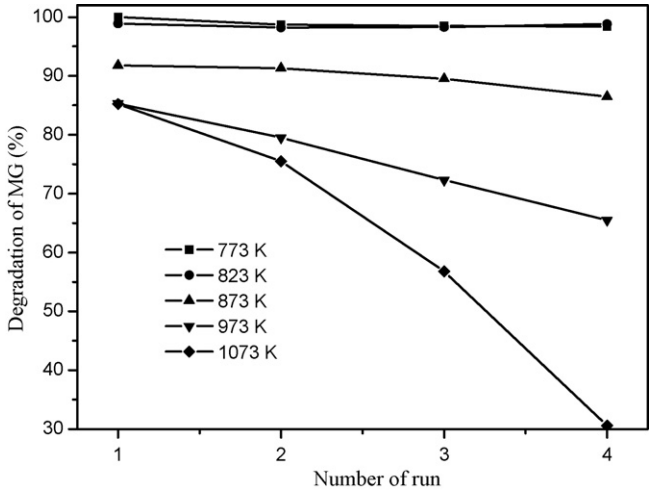

Fig. 12. Evaluation of the stability of the synthesized Ni,La-STO-1.0 series photocatalysts calcined at different temperature.

at 773 K was more than 98% even after 4 runs. However, an evident decrease of activity for catalyst calcined at higher temperature was observed. This may be due to the increase in hydrophobic property for the recycled catalysts, on which the static contact angle of water increases from 1° to >140° (measured on a contact angle analyzer (OCA-30)) after four runs, which makes most of recycled catalysts floated on the MG solution, resulting in an insufficient interaction between the catalysts and MG.

4. Conclusions

It was found that the calcination temperature strongly affects not only the structural properties and the vis-light photocatalytic activities but also the stability of the synthesized photocatalysts. The photocatalytic activities of the synthesized photocatalysts decreased with increasing calcination temperature due to the decrease in specific surface area, pore volume and initial adsorption rate as well as the large lattice distortion. The catalysts calcined at lower temperatures were more stable. A broad absorption tail in visible region was observed after co-doping of Ni and La. Although the nondoped $SrTiO_3$ shows a high activity due to dye-sensitization, co-doping of Ni and La did enhance the vis-light activity, especially for the catalysts calcined at high temperature. Moreover, the optimal doping amount of Ni and La is 1.0%. The photocatalytic activities of all synthesized photocatalysts are found to be greatly superior to that of the commercial P25 under visible light irradiation. Therefore, it is possible that the synthesized photocatalysts will be of great value to the efficient utilization of solar energy and will be used for various applications, such as self-cleaning, water contaminants degradation and air purification.

Acknowledgements

The research work is supported by National Natural Science Foundation of China (no. 20773069), The National Key Technologies R&D Program of China (2006BAC02A12) and Key Technologies R&D Program of Tianjin China (07ZCGYSH02000).

References

[1] S. Song, L. Xu, Z. He, H. Ying, J. Chen, X. Xiao, B. Yan, Photocatalytic degradation of C.I. Direct Red 23 in aqueous solutions under UV irradiation using $SrTiO_3/CeO_2$ composite as the catalyst, J. Hazard. Mater. 152 (2008) 1301–1308.
[2] Y. Lv, K. Shi, Y. Zhang, S. He, X. Guo, Z. Du, H. Chen, C. Zhang, B. Zhang, The characterization of Sr-doped nanocrystal grain microspheres and photodegradation of KN-R dye, Catal. Commun. 9 (2008) 557–562.
[3] M. Miyauchi, A. Nakajima, A. Fujishima, K. Hashimoto, T. Watanabe, Photoinduced surface reactions on TiO_2 and $SrTiO_3$ films: photocatalytic oxidation and photoinduced hydrophilicity, Chem. Mater. 12 (2000) 3–5.
[4] T. Puangpetch, T. Sreethawong, S. Yoshikawa, S. Chavadej, Synthesis and photocatalytic activity in methyl orange degradation of mesoporous-assembled $SrTiO_3$ nanocrystals prepared by sol–gel method with the aid of structure-directing surfactant, J. Mol. Catal. A: Chem. 287 (2008) 70–79.
[5] Y. Han, D.H. Chen, L. Zhang, Nanocrystallized SrHA/SrHA–$SrTiO_3$/$SrTiO_3$–TiO_2 multilayer coatings formed by micro-arc oxidation for photocatalytic application, Nanotechnology 19 (2008) 335705–335707.
[6] D. Wang, T. Kako, J. Ye, Efficient photocatalytic decomposition of acetaldehyde over a solid–solution perovskite $(Ag_{0.75}Sr_{0.25})(Nb_{0.75}Ti_{0.25})O_3$ under visible-light irradiation, J. Am. Chem. Soc. 130 (2008) 2724–2725.
[7] D. Wang, T. Kako, J. Ye, New series of solid-solution semiconductors $(AgNbO_3)_{1-x}(SrTiO_3)_x$ with modulated band structure and enhanced visible-light photocatalytic activity, J. Phys. Chem. C 113 (2009) 3785–3792.
[8] Y. Sasaki, A. Iwase, H. Katoa, A. Kudo, The effect of co-catalyst for Z-scheme photocatalysis systems with an Fe^{3+}/Fe^{2+} electron mediator on overall water splitting under visible light irradiation, J. Catal. 259 (2008) 133–137.
[9] K. Domen, A. Kudo, T. Onishi, N. Kosugi, H. Kuroda, Photocatalytic decomposition of water into hydrogen and oxygen over nickel(II) oxide-strontium titanate ($SrTiO_3$) powder. 1. Structure of the catalysts, J. Phys. Chem. 90 (1986) 292–295.
[10] K. Sayama, K. Mukasa, R. Abe, Y. Abe, H. Arakawa, A new photocatalytic water splitting system under visible light irradiation mimicking a Z-scheme mechanism in photosynthesis, J. Photochem. Photobiol. A: Chem. 148 (2002) 71–77.
[11] J.W. Liu, G. Chen, Z.H. Li, Z.G. Zhang, Electronic structure and visible light photocatalysis water splitting property of chromium-doped $SrTiO_3$, J. Solid State Chem. 179 (2006) 3704–3708.
[12] K. Domen, S. Naito, T. Onishi, K. Tamaru, M. Soma, Study of the photocatalytic decomposition of water vapor over a nickel (II) oxide-strontium titanate ($SrTiO_3$) catalyst, J. Phys. Chem. 86 (1982) 3657–3661.
[13] R. Asahi, T. Morikawa, K. Aoki, Y. Taga, Visible-light photocatalysis in nitrogen-doped titanium oxides, Science 293 (2001) 269–271.
[14] H. Irie, Y. Watanabe, K. Hashimoto, Nitrogen-concentration dependence on photocatalytic activity of $TiO_{2-x}N_x$ powders, J. Phys. Chem. B 107 (2003) 5483–5486.
[15] T. Umebayashi, T. Yamaki, S. Tanaka, K. Asai, Visible light-induced degradation of methylene blue on S-doped TiO_2, Chem. Lett. 32 (2003) 330–331.
[16] T. Ohno, T. Mitsui, M. Matsumura, Photocatalytic activity of S-doped TiO2 photocatalyst under visible light, Chem. Lett. 32 (2003) 364–365.
[17] T. Ohno, T. Tsubota, Y. Nakamura, K. Sayama, Preparation of S, C cation-codoped $SrTiO_3$ and its photocatalytic activity under visible light, Appl. Catal. A: Gen. 288 (2005) 74–79.
[18] H. Irie, Y. Maruyama, K. Hashimoto, Ag^+- and Pb^{2+}-doped SrTiO3 photocatalysts. A correlation between band structure and photocatalytic activity, J. Phys. Chem. C 111 (2007) 1847–1852.
[19] E. Borgarello, J. Kiwi, M. Gratzel, E. Pelizzetti, M. Visca, Visible light induced water cleavage in colloidal solutions of chromium-doped titanium dioxide particles, J. Am. Chem. Soc. 104 (1982) 2996–3002.
[20] N. Sepone, D. Lawless, J. Disdier, J.M. Hermann, Spectroscopic, photoconductivity, and photocatalytic studies of TiO_2 colloids: naked and with the lattice doped with Cr^{3+}, Fe^{3+}, and V^{5+} cations, Langmuir 10 (1994) 643–652.
[21] W. Choi, A. Termin, M. Hoffmann, The role of metal ion dopants in quantum-sized TiO_2: correlation between photoreactivity and charge carrier recombination dynamics, J. Phys. Chem. 98 (1994) 13669–13679.
[22] I. Nakamura, N. Negishi, S. Kutsuna, T. Ihara, S. Sugihara, K. Takeuchi, Role of oxygen vacancy in the plasma-treated TiO_2 photocatalyst with visible light activity for NO removal, J. Mol. Catal. A: Chem. 161 (2000) 205–212.

[23] K. Domen, A. Kudo, T. Onishi, Mechanism of photocatalytic decomposition of water into H_2 and O_2 over NiO–$SrTiO_3$, J. Catal. 102 (1986) 92–98.
[24] R. Niishiro, H. Kato, A. Kudo, Nickel and either tantalum or niobium-codoped TiO_2 and $SrTiO_3$ photocatalysts with visible-light response for H_2 or O_2 evolution from aqueous solutions, Phys. Chem. Chem. Phys. 7 (2005) 2241–2245.
[25] H. Kato, A. Kudo, Visible-light-response and photocatalytic activities of TiO_2 and $SrTiO_3$ photocatalysts codoped with antimony and chromium, J. Phys. Chem. B 106 (2002) 5029–5034.
[26] T. Ishii, H. Kato, A. Kudo, H_2 evolution from an aqueous methanol solution on $SrTiO_3$ photocatalysts codoped with chromium and tantalum ions under visible light irradiation, J. Photochem. Photobiol. A: Chem. 163 (2004) 181–186.
[27] M. Sathish, R.P. Viswanath, Photocatalytic generation of hydrogen over mesoporous CdS nanoparticle: effect of particle size, noble metal and support, Catal. Today 129 (2007) 421–427.
[28] S.-K. Lee, P.K.J. Robertson, A. Mills, D. McStay, N. Elliott, D. McPhail, The alteration of the structural properties and photocatalytic activity of TiO_2 following exposure to non-linear irradiation sources, Appl. Catal. B: Environ. 44 (2003) 173–184.
[29] H. Tada, S. Tsuji, S. Ito, Photodeposition of prussian blue films on TiO_2: additive effect of methanol and influence of the TiO2 crystal form, J. Colloid Interface Sci. 239 (2001) 196–199.
[30] K. Inumaru, M. Murashima, T. Kasahara, S. Yamanaka, Enhanced photocatalytic decomposition of 4-nonylphenol by surface-organografted TiO_2: a combination of molecular selective adsorption and photocatalysis, Appl. Catal. B: Environ. 52 (2004) 275–280.
[31] E. Otsuka, K. Kurumada, A. Suzuki, S. Matsuzawa, K. Takeuchi, An application of transparent mesoporous bulk silica to a titanium dioxide photocatalyst with adsorption and decomposition functions, J. Sol–Gel Sci. Technol. 46 (2008) 71–78.
[32] C. Kang, L. Jing, T. Guo, H. Cui, J. Zhou, H. Fu, Mesoporous SiO_2-modified nanocrystalline TiO_2 with high anatase thermal stability and large surface area as efficient photocatalyst, J. Phys. Chem. C 113 (2009) 1006–1013.
[33] J. Zhang, M.J. Li, Z.C. Feng, J. Chen, C. Li, UV Raman spectroscopic study on TiO_2. I. Phase transformation at the surface and in the bulk, J. Phys. Chem. B 110 (2006) 927–935.
[34] H. Yamashita, Y. Horiuchi, S. Imaoka, S. Nishio, N. Nishiyama, K. Mori, Surface hydrophilic–hydrophobic property on transparent mesoporous silica thin films containing chromium oxide single-site photocatalyst, Catal. Today 132 (2008) 146–152.
[35] P. Gorska, A. Zaleska, E. Kowalska, T. Klimczuk, J.W. Sobczak, E. Skwarek, W. Janusz, J. Hupka, TiO_2 photoactivity in vis and UV light: the influence of calcination temperature and surface properties, Appl. Catal. B: Environ. 84 (2008) 440–447.
[36] K. Gomann, G. Borchardt, M. Schulz, A. Gomann, W. Maus-Friedrichs, B. Lesage, O. Kaitasov, S. Hoffmann-Eiferte, T. Schneller Sr., Diffusion in undoped and La-doped $SrTiO_3$ single crystals under oxidizing conditions, Phys. Chem. Chem. Phys. 7 (2005) 2053–2060.
[37] F. Wei, L. Ni, P. Cui, Preparation and characterization of N-S-codoped TiO_2 photocatalyst and its photocatalytic activity, J. Hazard. Mater. 156 (2008) 135–140.
[38] P. He, H.-R. Cheng, Y. Le, J.-F. Chen, Preparation and characterization of nanosized $Sr_{0.7}Ca_{0.3}TiO_3$ crystallines by low temperature aqueous synthesis method, Mater. Lett. 62 (2008) 2157–2160.
[39] E.R. Leite, C.M.G. Sousa, E. Longoa, J.A. Varela, Influence of polymerization on the synthesis of $SrTiO_3$: part I. Characteristics of the polymeric precursors and their thermal decomposition, Ceram. Int. 21 (1995) 143–152.
[40] D. Wang, J. Ye, T. Kako, T. Kimura, Photophysical and photocatalytic properties of $SrTiO_3$ doped with Cr cations on different sites, J. Phys. Chem. B 110 (2006) 15824–15830.
[41] Y. Qin, G. Wang, Y. Wang, Study on the photocatalytic property of La-doped CoO/$SrTiO_3$ for water decomposition to hydrogen, Catal. Commun. 8 (2007) 926–930.
[42] B.W. Faughnan, Photochromism in transition-metal-doped $SrTiO_3$, Phys. Rev. B 4 (1971) 3623–3636.
[43] M. Dogan, H. Abak, M. Alkan, Adsorption of methylene blue onto hazelnut shell: kinetics, mechanism and activation parameters, J. Hazard. Mater. 164 (2009) 172–181.
[44] C.J. Stephanson, G.P. Flanagan, Antioxidant capacity of silica hydride: a combinational photosensitization and fluorescence detection assay, Free Radic. Biol. Med. 35 (2003) 1129–1137.
[45] C. Galindo, P. Jacques, A. Kalt, Photooxidation of the phenylazonaphthol AO20 on TiO_2: kinetic and mechanistic investigations, Chemosphere 45 (2001) 997–1005.
[46] M. Miyauchi, M. Takashio, H. Tobimastsu, Photocatalytic activity of $SrTiO_3$ codoped with nitrogen and lanthanum under visible light illumination, Langmuir 20 (2004) 232–236.